

Review—Importance of Atmospheric Gas Selection in Metal Additive Manufacturing: Effects on Spatter, Microstructure, and Mechanical Properties*¹

Hiroki Amano^{1,2,*2}, Takuya Ishimoto^{2,3,4} and Takayoshi Nakano^{2,3}

¹TAIYO NIPPON SANZO Corporation, Tokyo 142-8558, Japan

²Division of Materials and Manufacturing Science, Graduate School of Engineering, Osaka University, Suita 565-0871, Japan

³Anisotropic Design & Additive Manufacturing Research Center, Osaka University, Suita 565-0871, Japan

⁴Aluminium Research Center, University of Toyama, Toyama 930-8555, Japan

In metal additive manufacturing, it is possible to control the microstructure and the associated mechanical and chemical properties of metal products over a wide range. For example, in laser powder bed fusion (L-PBF), the laser process parameters are considered critical for the fabrication of functional parts. However, the effect of atmospheric gas on L-PBF has not yet been comprehensively documented. In L-PBF, gas flow is used to remove spatter and fumes, preventing degradation of quality due to laser attenuation and spatter contamination of the fabricated product. Thus, the use of atmospheric gas is inevitable in fabrication via L-PBF. In this review, we focus on the use of atmospheric gas in L-PBF, explain the effects of atmospheric gas on the microstructure and mechanical properties of fabricated products, and describe the importance of selecting the right atmospheric gas. [doi:10.2320/matertrans.MT-MLA2022005]

(Received June 3, 2022; Accepted June 12, 2022; Published September 16, 2022)

Keywords: additive manufacturing, laser powder bed fusion, atmosphere, gas, cooling rate

1. Introduction

Metal additive manufacturing (AM) is a type of metal processing technology that enables accurate manufacturing of structures with arbitrary shapes.^{1–3} Recent studies have established AM technology as a process that can control not only the shape of metallic materials, but also the microstructures and the resulting mechanical properties. Typical examples of metal AM methods include laser powder bed fusion (L-PBF) and electron beam powder bed fusion (EB-PBF).^{4–13} Among the microstructural characteristics of metallic materials, crystallographic texture is an important factor that confers anisotropy to their mechanical properties. For example, fabricated products with preferential crystal orientation exhibit anisotropy of mechanical and chemical properties, such as Young's modulus,^{5,14} yield stress, elongation,¹⁵ fatigue resistance,¹⁶ creep resistance,¹⁷ and oxidation resistance.¹⁸ In addition, metallic parts with various structures and crystal orientations can be realized by changing the thermal gradient at the solid–liquid interface and the migration direction of the solid–liquid interface by modifying various process parameters (e.g., the heat source power, scan speed, and scan strategy).^{19–23} PBF is anticipated to be used in various industrial fields, and their application in a wide range of disciplines is being considered. Research and development are progressing in various fields of industrial manufacturing, including aircraft-related parts and medical equipment, and some fields have already begun to put these PBF methods into practical use.²⁴

In EB-PBF, fabrication is performed in vacuum (generally, a helium (He) gas atmosphere on the order of 10^{-1} Pa is used to suppress smoke); meanwhile, in L-PBF, gas flow is used to remove spatter and fumes. Considering that the gas should be inert, argon (Ar) or nitrogen (N₂) is typically employed

depending on the metal. When a highly reactive metal is used, N₂ reacts at high temperatures. In such cases, Ar is selected. By removing by-products, such as spatter and fumes, quality degradation due to laser attenuation and spatter contamination of the fabricated products can be prevented. Therefore, the use of atmospheric gas is unavoidable during the L-PBF fabrication. Because a gaseous atmosphere is required anyway, our research group is attempting to actively utilize the gas for metallographic structure control.

When focusing on the physical characteristics of the gases themselves, as shown in Table 1, there is no significant difference in the thermal conductivity or density between Ar and N₂ generally used in L-PBF.²⁵ Conversely, He has a lower density, higher thermal conductivity, and higher cooling capacity than Ar or N₂.²⁵ Therefore, the focus is on the high cooling capacity of He and the possibility of controlling the microstructure and mechanical properties using He. In general, the characteristics of the fabricated parts in PBF depend on the input energy density E defined by eq. (1).

Table 1 Gas properties used in the simulation (standard ambient temperature and pressure).²⁵

	Argon	Nitrogen	Helium
Relative molecular mass, M_r	39.94	28.016	4.003
Density, $\rho / \text{kg}\cdot\text{m}^{-3}$	1.6339	1.1452	0.16353
Thermal conductivity, $\lambda / \text{mW}\cdot\text{m}^{-1}\text{K}^{-1}$	17.746	25.835	155.31
Viscosity, $\mu / \mu\text{Pa}\cdot\text{s}$	22.624	17.805	19.846
Specific heat, $C_p / \text{kJ}\cdot\text{kg}^{-1}\text{K}^{-1}$	0.52156	1.0413	5.193

*¹This Paper was Originally Published in Japanese in J. JILM 72 (2022) 220–226. The title was changed due to the addition of “Review—”.

*²Corresponding author, E-mail: amanoh.qtg@tn-sanso.co.jp

$$E = P/(vsh) \quad (1)$$

where P is the laser power, v is the scanning speed, s is the scan pitch, and h is the layer thickness. However, the effect of atmospheric gas cooling, which is not expressed by eq. (1), is discussed in this study.

2. Suppression of Spatter by Atmospheric Gas

Defects formed during the fabrication process are a major issue in L-PBF. Defect formation negatively affects the mechanical and chemical properties of the products and introduces uncertainty in the quality control of the fabricated products, thus hindering the practical application of AM technology in various industries.²⁶⁾ Spatters are one of the main causes of defect formation.^{27,28)} The formation of spatter reduces the energy efficiency of the laser as the spatter lies on the laser path.^{29–31)} Furthermore, it is scattered in the powder layer before laser irradiation and incorporated into the fabricated products, which affect their mechanical properties.³²⁾ It has been reported that the oxygen content of spatter generated during Ti-alloy fabrication is approximately twice that of the raw material powder as a result of oxidation by heat.³³⁾ In L-PBF, the unmelted powder is typically collected and reused. However, if the recovered powder contains spatter, the oxygen concentration of the fabricated products may increase unexpectedly during the next fabrication process. Therefore, suppression of spatter is necessary for the quality control of L-PBF. In previous studies, laser process parameters were studied in an attempt to suppress spatter. For example, spatter can be suppressed by decreasing the laser power or increasing the scanning speed.³⁴⁾ Spatters can also be suppressed by changing the oscillation method of the laser itself from continuous to pulse.³⁵⁾ However, when considering microstructural control of fabricated parts, the range of optimal laser process parameters to obtain the desired microstructure is limited and does not always meet the conditions necessary for suppressing spatter. Therefore, it is important to suppress spatter using atmospheric gas during fabrication, in addition to using laser process parameters.

Recent studies have attempted to control spatter using atmospheric gas. In Ti–6Al–4V alloys, the effect of oxygen (O_2) contained in the atmosphere during the fabrication process on the generation of spatter and the effect of changing the atmospheric gas to He gas has been reported using single-layer basic evaluation equipment that imitates L-PBF.³⁶⁾ Figures 1 and 2 show the graphs of the state of spatter generation and the weight of the recovered spatter when O_2 , which is an impurity component, is added to He in addition to the conventional atmospheric gas Ar. As the O_2 concentration in the Ar and He atmospheres increased, the amount of spatter increased significantly; with a He atmosphere, the generation of spatter was more suppressed compared to an Ar atmosphere. Spatter commonly occurs when the atmosphere at the laser-irradiated part becomes instantaneously heated and expands, and the resulting updraft stirs up the metal powder, which is also generated by the reactionary pressure associated with the extreme expansion of the gas phase.^{31,37)} That is, the temperature rise

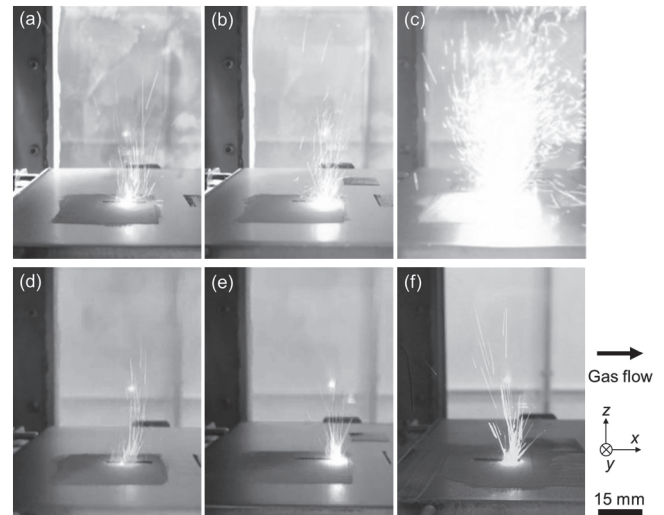


Fig. 1 Spatter generation in (a)–(c) Ar and (d)–(f) He atmosphere using single-layer basic evaluation equipment as a function of oxygen (O_2) concentration in the atmosphere. Oxygen concentrations of less than 50 ppm (a), (d), 1.0% (b), (e), and 5.0% (c), (f) were used. Modified from Ref. 36).

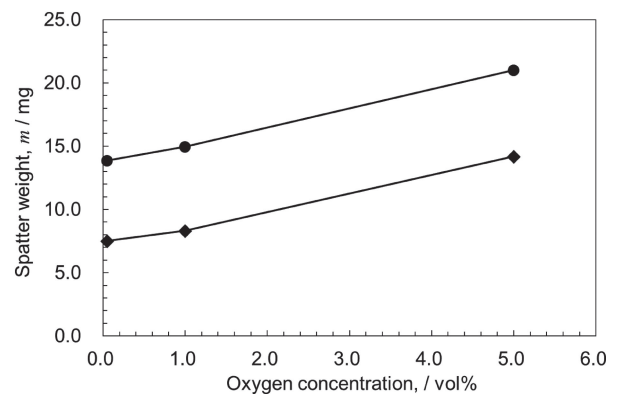


Fig. 2 Change in spatter generated with change in O_2 concentration in Ar and He atmospheres using single-layer basic evaluation equipment. Modified from Ref. 36).

at the laser-irradiated part leads to the occurrence of a spatter.

The increase in spatter associated with an increase in O_2 concentration in the atmosphere was due to the convection direction of the molten metal in the melt pool. Convection occurs in the direction of lower to higher surface tension. The surface tension of Ti decreases as the dissolved oxygen in Ti increases.³⁸⁾ At the periphery of the melt pool, the exposure time to the atmosphere was longer than that at the center (laser irradiation). Therefore, the amount of solute oxygen increased and the surface tension decreased, resulting in convection toward the center. That is, the high-temperature molten metal flows into the laser-irradiated part, and the temperature increases further. Convection toward the center increased as the O_2 concentration in the atmosphere increased. Consequently, the amount of spatter generated may also increase.

The suppression of spatter generation in the He atmosphere was due to the temperature drop in the laser-irradiated part. By using He gas as the fabrication atmosphere, the heat

transfer coefficient between the fabricated product and the gas-phase atmosphere in the laser irradiation area was significantly changed. The heat transfer coefficient h can be expressed using the following equations.³⁹⁾

$$Re = \rho ul / \mu \quad (2)$$

$$Pr = \mu C_p / \lambda \quad (3)$$

$$Nu = 0.664 Re^{1/2} Pr^{1/3} \quad (4)$$

$$Nu = hl / \lambda \quad (5)$$

where Re is the Reynolds number, ρ is the fluid density, u is the flow velocity, l is the representative length, μ is the absolute viscosity, Pr is the Prandtl number, λ is the thermal conductivity, C_p is the specific heat at constant pressure, and Nu is the Nusselt number. The numerical values listed in Table 1 were used to determine the physical characteristics of the gas. When the flow velocity on the base plate is the same for both Ar and He gases, the heat transfer coefficient of the He atmosphere in the laser irradiation area is approximately 2.7 times that of the Ar atmosphere. Therefore, when He is used, heat dissipation from the surface of the fabricated products to the gas phase is promoted. Therefore, when using He gas for the fabrication atmosphere, as shown in Fig. 3, the cooling rate of the laser-irradiated part was faster compared to Ar gas, and the generation of spatter was suppressed by reducing the expansion of the atmosphere. In fact, by changing the atmospheric gas type to He not only in single-layer basic evaluation equipment, but also in the actual L-PBF apparatus, the occurrence of spatter is significantly suppressed, as shown in Fig. 4. Therefore, the decrease in O_2 concentration in the atmosphere and application of He gas is expected to lead to the expansion of the application of L-PBF based on the improvement in quality of the fabricated products, as well as the recycled powder.

3. Effect of Atmospheric Gas on Various Characteristics of Fabricated Products

Recent studies have reported the effects of changing atmospheric gases on the fabricated products for a variety of metals. Comparisons have been made when the atmospheric gas is changed using the same laser process parameters, and studies have been conducted that utilize the cooling performance of the atmospheric gas.

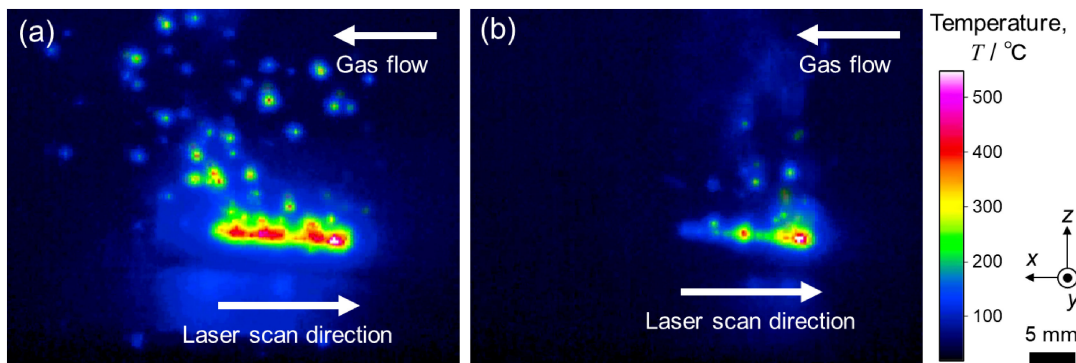


Fig. 3 Thermal images during laser irradiation in (a) Ar and (b) He atmospheres using single-layer basic evaluation equipment. Modified from Ref. 36).

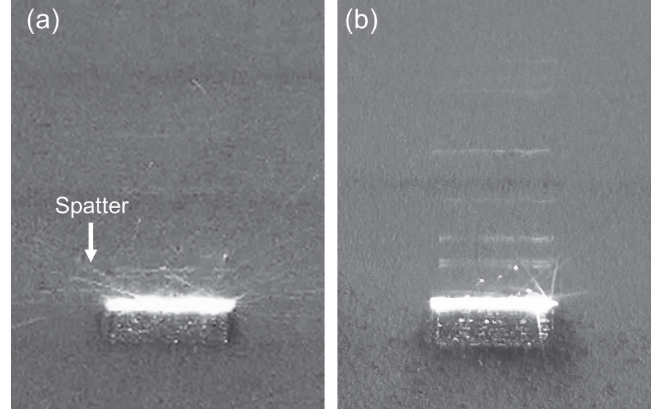


Fig. 4 Spatter generation behavior in (a) Ar and (b) He atmospheres using an actual L-PBF apparatus. Modified from Ref. 36).

3.1 Effect of He atmosphere on L-PBF fabrication

While examining the effects of atmospheric gases, inert He is often used as a comparison for Ar and N_2 . In L-PBF fabrication of the AlSi10Mg alloy, the dependence of the surface roughness and relative density of the fabricated products on the atmospheric species was confirmed, and good results were obtained using an Ar atmosphere. This is because the atmospheric gas species change the vector of the velocity distribution of the evaporative metal. Under a He atmosphere, the vector of the velocity distribution of the evaporated metal is horizontal or downward, and a non-uniform recoil pressure is applied to the free surface of the melt pool. Under an N_2 atmosphere, the vector of the velocity distribution of the evaporative metal tends to point toward the interaction area between the laser and the powder, and a stack of materials is generated. Conversely, in an Ar atmosphere, the vector of the velocity distribution of the evaporated metal points upward and a uniform recoil pressure is applied to the free surface of the melt pool. Therefore, the depth of the melt pool and the pressure on the surface of the melt pool are more stable when using Ar compared to He and N_2 atmospheres.⁴⁰⁾ In Al-12Si alloys, Ar and N_2 atmospheres improve the mechanical properties; meanwhile a He atmosphere results in reduced ductility. This is due to the formation of fine pore clusters inside the fabricated parts; however, the factors that form pore clusters have not been elucidated.⁴¹⁾ In the fabrication of Ti-6Al-4V alloy, a high relative density was obtained by changing the laser power and scanning speed in

an atmosphere containing He. Furthermore, the use of a He-containing atmosphere enables the scanning speed to be faster than that in Ar, and it is possible to decrease the building time. This is because the by-products during the fabrication process are suppressed, and the reduction of the laser energy input is suppressed in a He-containing atmosphere.⁴²⁾ When the fabrication process parameters are the same, high relative densities were obtained in both Ar and He atmosphere.⁴³⁾

3.2 Microstructural control by L-PBF focusing on the high cooling performance of He gas

Research has focused on the cooling properties of He gas in L-PBF. The cooling rate has a significant effect on the microstructure. For example, the microstructures of Ti-6Al-4V alloy formed by L-PBF and EB-PBF depend on the cooling rate of the two methods and differ greatly; that is, the L-PBF method, which enables a higher cooling rate, produces a finer microstructure.⁴⁴⁻⁴⁶⁾ This difference in cooling rate is also caused by the utilization of He.⁴³⁾

When He was used instead of Ar as the atmospheric gas, the Vickers hardness, 0.2% proof strength, and ultimate strength of the products were improved, even with the same laser irradiation conditions, as shown in Figs. 5 and 6. Furthermore, in the Vickers hardness shown in Fig. 5, the center of the fabricated products exhibited a higher value than the edge. This depends on the grain size as the Hall-Petch rule holds between Vickers hardness and grain size.⁴³⁾ As shown in Fig. 7, the structure inside the fabricated parts was mostly composed of needle-shaped α' martensite in both atmospheres.⁴⁷⁾ This is because the cooling rate with L-PBF is 410 K/s⁴⁸⁾ or higher, which is the lower limit of the martensitic transformation. In fact, in the L-PBF method, cooling rates of approximately 10^5 to 10^7 K/s are observed.²¹⁾

The α' martensite grain size in the He atmosphere was finer than that in the Ar atmosphere. Furthermore, the center of the fabricated products had a finer grain size than the edge. The mechanical properties of the fabricated products differ significantly depending on the atmospheric gas, and the use of He gas results in excellent mechanical properties due to the refinement of the α' martensite grain size.

To clarify such changes in the grain size, it is necessary to analyze the thermal history during solidification and phase transformation. The melting and solidification processes

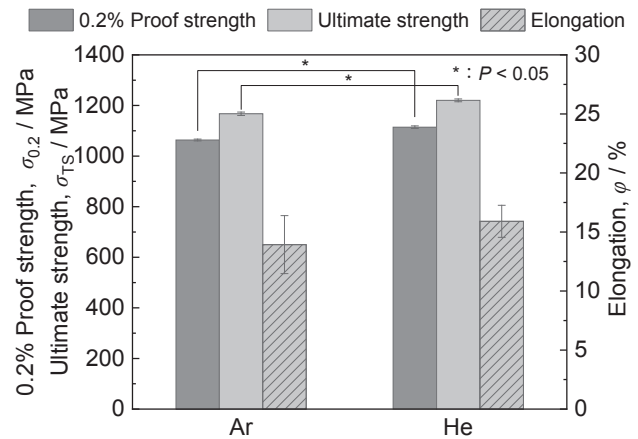


Fig. 6 Mechanical properties of products fabricated under Ar and He atmospheres. Modified from Ref. 43).

during actual laser irradiation occur extremely rapidly; therefore, utilizing computer simulations for the analysis of melting and solidification behavior is useful.⁴⁹⁻⁵¹⁾ As shown in Fig. 8, reciprocating scanning of the laser causes a periodic temperature rise, even after the molten metal solidifies. However, the solidified part does not reach the α/β phase transition temperature (975°C)⁵²⁾ or the martensitic transformation start temperature (M_s) (800°C).⁵³⁾ The time required for the entire solidification and cooling process at the edges of the fabricated products was approximately twice than that at the center of the fabricated products, and the cooling rate during solidification differed significantly (Fig. 8). When comparing the cooling rate of the center of the products fabricated under He and Ar atmospheres, as shown in Fig. 9, the cooling rate reaches $\sim 7 \times 10^6$ K/s immediately after the laser passes, and at temperatures near M_s , the cooling rate increases in the He atmosphere. These results suggest that heat dissipation from the surface of the fabricated products to the gas phase was promoted. Therefore, this thermal history is the cause of the difference in the α' martensite grain size. The refinement of the microstructure when using a He atmosphere has also been reported for austenitic stainless steel 316L (316L SS).⁵⁴⁾ As shown in Fig. 10, in the cellular microstructure of the melt pool inside the products, the cell width was smaller in the He atmosphere than in the Ar atmosphere. For 316L SS, the cooling rate can be estimated from the cell width using eq. (6).⁵⁵⁾

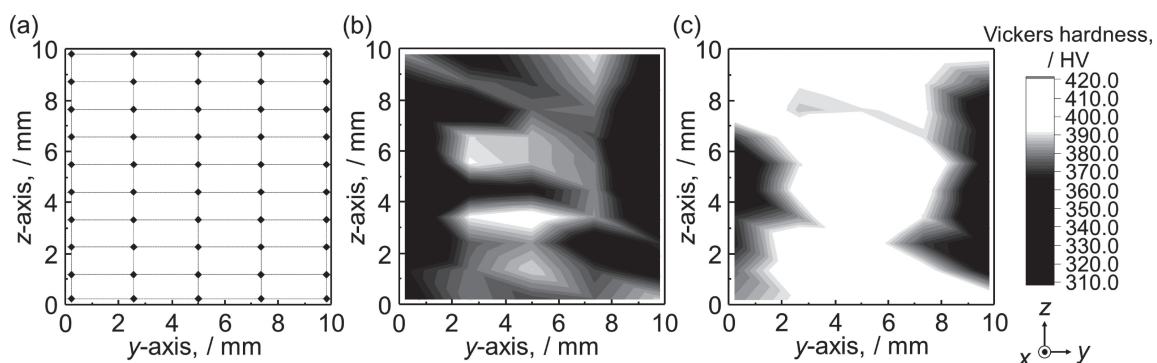


Fig. 5 (a) Vickers hardness measurement points. Distribution of Vickers hardness in the products fabricated under (b) Ar and (c) He atmospheres. Modified from Ref. 43).

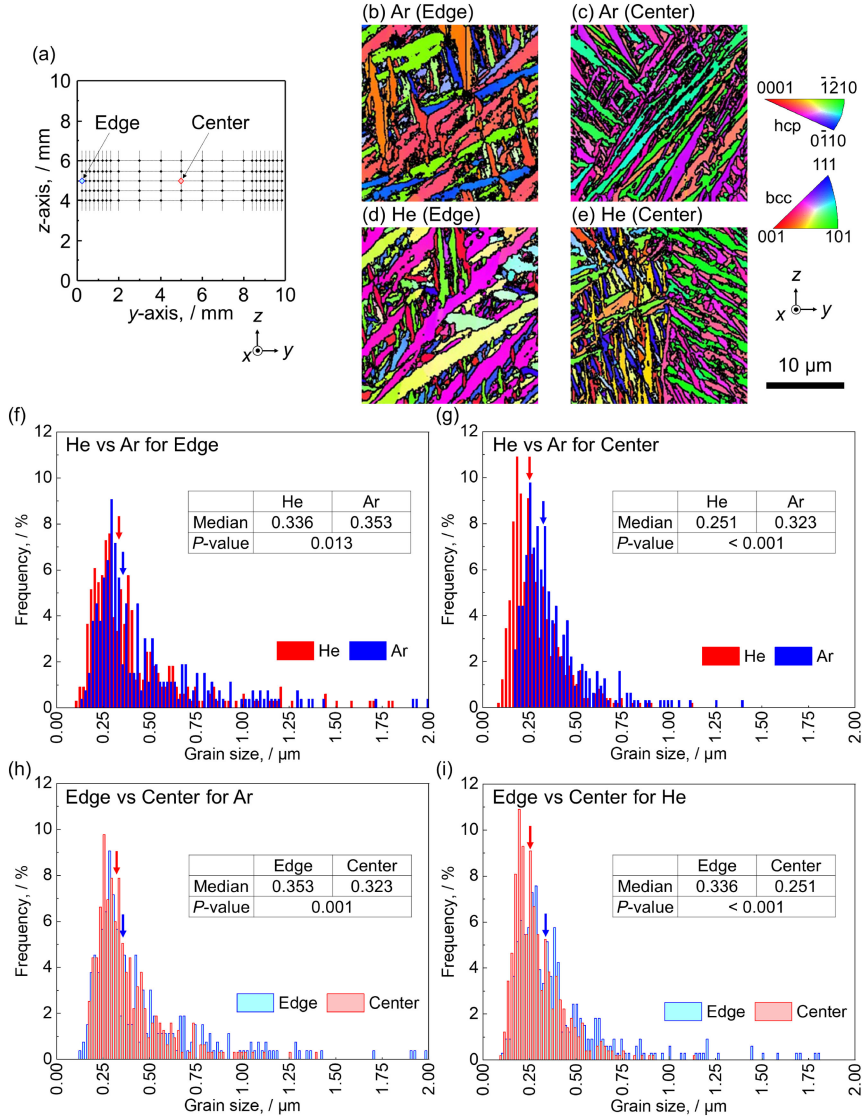


Fig. 7 (a) Measurement points in the fabricated products. Crystallographic orientation map in the z direction for the (b), (d) edge and (c), (e) center of the products fabricated under (b), (c) Ar and (d), (e) He atmospheres. (f)–(i) Comparisons of the α' martensite grain size. Arrows indicate the median particle size. Modified from Ref. 43).

$$d \text{ (}\mu\text{m)} = 80\dot{T}^{-0.33} \quad (6)$$

where d is the cell width and \dot{T} is the cooling rate. The cell width was $0.305 \mu\text{m}$ in a He atmosphere and $0.354 \mu\text{m}$ in an Ar atmosphere, and the estimated cooling rates were $2.14 \times 10^7 \text{ K/s}$ and $1.37 \times 10^7 \text{ K/s}$, respectively. Therefore, the cooling rate obtained by fabrication in a He atmosphere is 1.5 times that of the cooling rate obtained by fabrication in an Ar atmosphere. The improvement in the cooling rate contributes to the suppression of the formation and growth of inclusions, and an improvement in the corrosion resistance of stainless steel.^{56–58)}

4. Future Potential for Atmospheric Gas Utilization in L-PBF

As mentioned previously, the atmospheric gas in L-PBF is an important factor influencing the L-PBF process, microstructure, and mechanical properties of the products. Furthermore, for atmospheric gas, in addition to the gas

type, the direction and velocity of the gas flow are also important.

Regarding the direction of gas flow, the spatter, fume, and plume generated during laser irradiation move along the same path as the laser irradiation when the laser scanning and gas flow directions match. Therefore, the laser energy is attenuated, and the quality of the product deteriorates because of poor melting and spatter contamination in the fabricated products.^{29–31)}

Regarding the gas flow velocity, if the flow velocity is too low, the quality of the fabricated parts deteriorates. This is because the laser energy is attenuated by the steam plume generated in the L-PBF process and the shape of the melt pool changes, resulting in an increase in the number of pores in the fabricated products.⁵⁹⁾ When the flow velocity is too high, the powder is blown off by the gas flow, and the thickness of the powder bed fluctuates, resulting in the deterioration of the quality of the fabricated products.⁶⁰⁾ That is, the stability of gas flow is indispensable for homogeneous fabrication. However, a fluid simulation using the finite

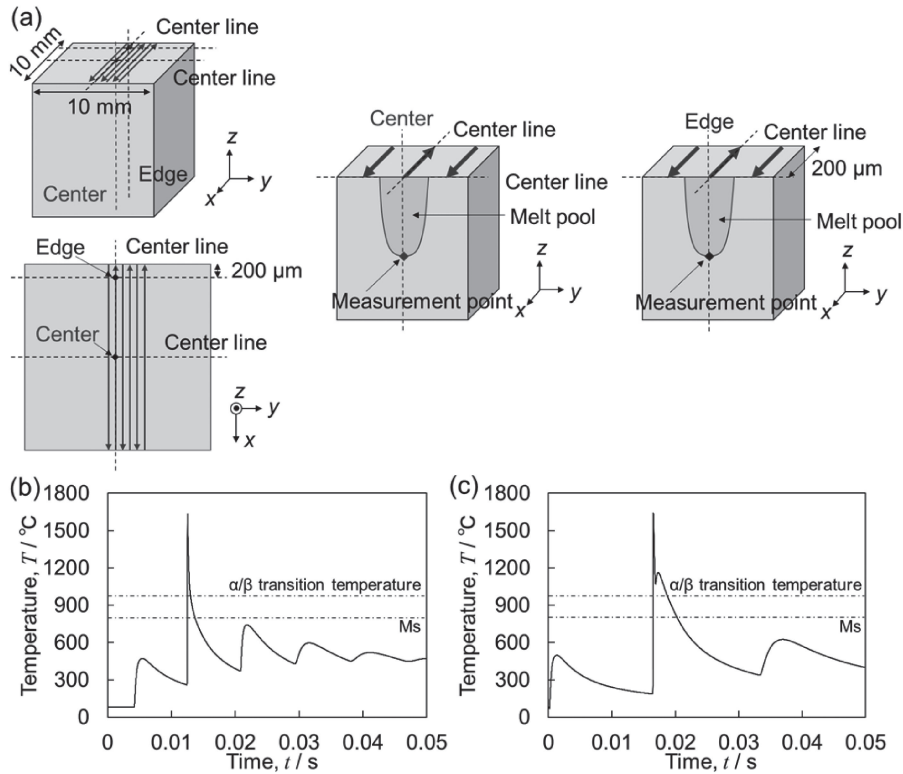


Fig. 8 (a) Analysis position of temperature simulation inside the model (center and edge). Temperature change at the (b) center and (c) edge under Ar atmosphere. The position where the melt pool depth is maximum was analyzed. Modified from Ref. 43).

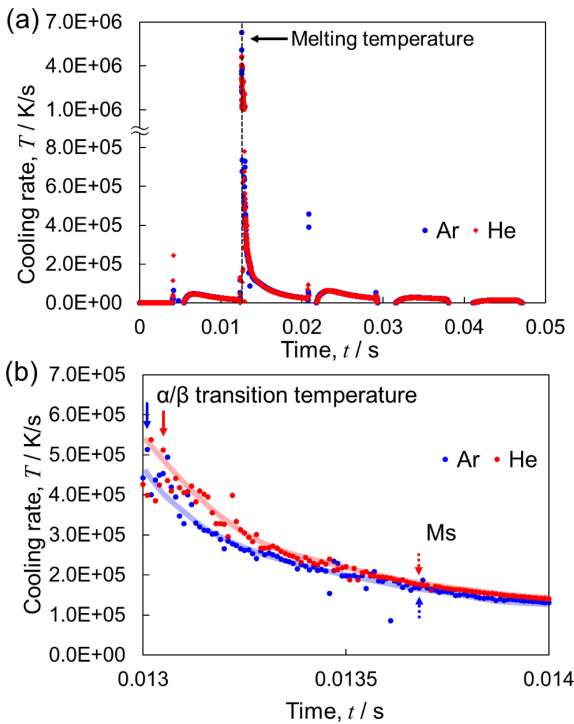


Fig. 9 (a) Changes in the cooling rate at the center (see Fig. 8(a)) in Ar and He atmospheres. (b) Enlarged view of the region showing α/β transus and Ms. Modified from Ref. 43).

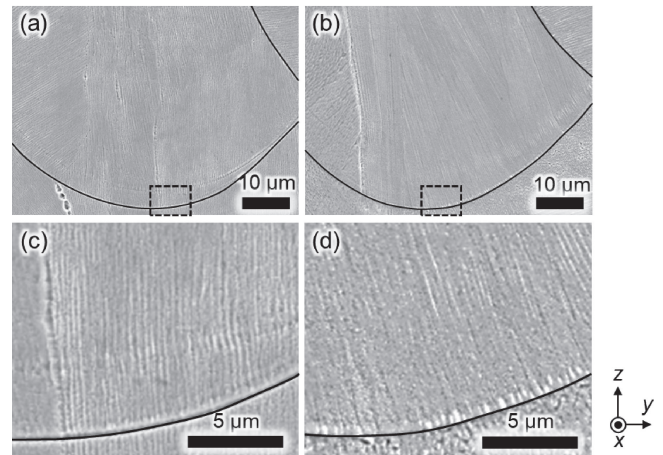


Fig. 10 Cellular microstructures of the products fabricated under (a) Ar and (b) He atmospheres. (c), (d) Enlarged view of the dashed rectangles in (a), (b). Black lines indicate contour of melt pool. Modified from Ref. 54).

volume method in an L-PBF apparatus shows that the flow velocity and direction of the atmospheric gas in the fabrication stage are widely distributed.⁴³⁾ As shown in Fig. 11, the non-uniformity of the gas flow is large in the red solid line frame representing the fabrication table,

particularly in the vicinity of the gas outlet and suction port. This suggests that the heat transfer coefficient and resulting microstructure of the fabricated products may depend on the position of the products placed on the fabrication table. Therefore, it is necessary to consider installing the base plate, for example, on the inside of the red dashed line, where the flow is uniform. Therefore, the method of supplying atmospheric gas is an important factor in terms of the quality of fabricated products. Further research is needed to elucidate the influence of atmospheric gas-related characteristics, such as gas type, flow rate, and flow path, during the L-PBF process to improve the quality of the fabricated parts and functionalize them.

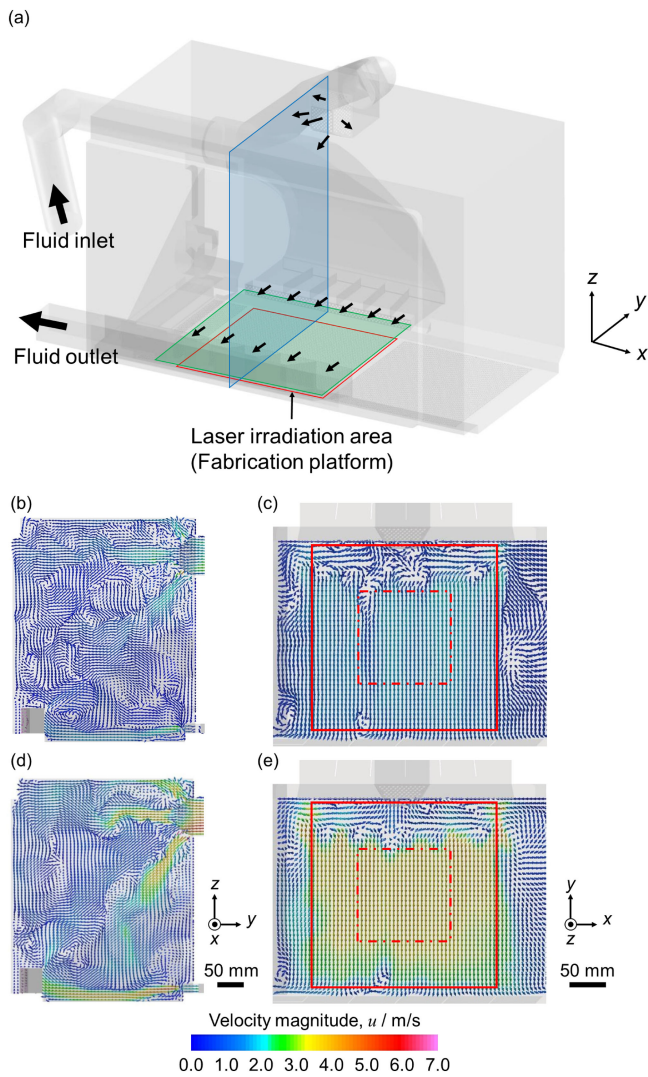


Fig. 11 (a) Calculation model for fluid simulation. The red frame indicates the laser irradiation area, while the blue frame and the green frame indicate the observation positions for (b), (d) and (c), (e), respectively. The distribution of fluid flow and flow velocity under (b), (c) Ar and (d), (e) He atmospheres are shown. The red dashed frame is the area where the flow is uniform. Modified from Ref. 43).

In addition, He gas may drastically change the microstructural characteristics of various metallic materials in the L-PBF process owing to its high cooling effect. For example, in high-entropy alloys, mechanical strength is significantly improved by forming a supersaturated solid solution via L-PBF.⁶¹⁾ Conversely, a high cooling rate suppresses precipitation of the strengthening phase, leading to a decrease in precipitation strengthening.^{62,63)} These changes in the properties of metallic materials as a result of the high cooling rate of L-PBF are expected to be improved and optimized by the careful selection of atmospheric gas species.

He gas is a non-renewable gas extracted from natural gas, and is a scarce resource. Therefore, the reuse of gas is crucial. However, the reuse of He gas is associated with problems such as gas pollution during atmospheric circulation in L-PBF fabrication⁶⁴⁾ and gas leakage from L-PBF equipment. Currently, the development of He purification/recycling technology is under consideration.^{65,66)} Therefore, in the future, the application of He gas to L-PBF can be realized by

employing suitable refining/recycling technology and improving L-PBF equipment, for example, by improving its airtightness.

5. Conclusion

Atmospheric gas is an important parameter in L-PBF, both for spatter and fume removal and for modifying the microstructure and related mechanical and chemical properties of fabricated parts by controlling the cooling rate during fabrication. The parameters related to atmospheric gas are indices that are not included in the energy density, which have traditionally been used as a controlling factor for product quality. Therefore, in the future, the application of He gas to L-PBF can be realized by applying an appropriate refining/recycling technology and improving L-PBF equipment, for example, by improving the airtightness. In the future, the active use and control of gas-related indices are expected to expand the control range of the microstructure and mechanical/chemical properties of L-PBF-fabricated metal products.

Acknowledgments

This work was supported by a Grant-in-Aid for Scientific Research (JP18H05254) from the Japan Society for the Promotion of Science (JSPS) and CREST-Nanomechanics: Elucidation of macroscale mechanical properties based on understanding nanoscale dynamics of innovative mechanical materials (Grant Number: JPMJCR2194) from the Japan Science and Technology Agency (JST). Part of this content was also supported by a 1st Frontier Research Grant from the Japan Institute of Metals.

REFERENCES

- 1) N. Aage, E. Andreassen, B.S. Lazarov and O. Sigmund: *Nature* **550** (2017) 84–86.
- 2) P. Wang, J. Song, M.L.S. Nai and J. Wei: *Addit. Manuf.* **33** (2020) 101088.
- 3) S. Liu and Y.C. Shin: *Mater. Des.* **164** (2019) 107552.
- 4) K. Cho, H. Kawabata, T. Hayashi, H.Y. Yasuda, H. Nakashima, M. Takeyama and T. Nakano: *Addit. Manuf.* **46** (2021) 102091.
- 5) T. Ishimoto, K. Hagihara, K. Hisamoto, S.-H. Sun and T. Nakano: *Scr. Mater.* **132** (2017) 34–38.
- 6) S.Y. Liu, H.Q. Li, C.X. Qin, R. Zong and X.Y. Fang: *Mater. Des.* **191** (2020) 108642.
- 7) K. Cho, R. Kobayashi, J.Y. Oh, H.Y. Yasuda, M. Todai, T. Nakano, A. Ikeda, M. Ueda and M. Takeyama: *Intermetallics* **95** (2018) 1–10.
- 8) K. Hagihara, T. Nakano, M. Suzuki, T. Ishimoto, Suyalatu and S.-H. Sun: *J. Alloy. Compd.* **696** (2017) 67–72.
- 9) T. Ishimoto, S. Wu, Y. Ito, S.-H. Sun, H. Amano and T. Nakano: *ISIJ Int.* **60** (2020) 1758–1764.
- 10) M. Higashi and T. Ozaki: *Mater. Des.* **191** (2020) 108588.
- 11) M.-S. Pham, B. Dovgvy, P.A. Hooper, C.M. Gourlay and A. Piglione: *Nat. Commun.* **11** (2020) 749.
- 12) N. Ikee, T. Ishimoto, A. Serizawa and T. Nakano: *Metall. Mater. Trans. A* **45** (2014) 4293–4301.
- 13) N. Ikee, T. Ishimoto and T. Nakano: *J. Alloy. Compd.* **639** (2015) 336–340.
- 14) S.-H. Lee, M. Todai, M. Tane, K. Hagihara, H. Nakajima and T. Nakano: *J. Mech. Behav. Biomed. Mater.* **14** (2012) 48–54.
- 15) J.J. Marattukalam, D. Karlsson, V. Pacheco, P. Beran, U. Wiklund, U. Jansson, B. Hjärvarsson and M. Sahlberg: *Mater. Des.* **193** (2020) 108852.

- 16) T.P. Gabb, J. Gayda and R.V. Miner: *Metall. Trans. A* **17** (1986) 497–505.
- 17) L.Y. Wang, Y.C. Wang, Z.J. Zhou, H.Y. Wan, C.P. Li, G.F. Chen and G.P. Zhang: *Mater. Des.* **195** (2020) 109042.
- 18) O. Gokcekaya, N. Hayashi, T. Ishimoto, K. Ueda, T. Narushima and T. Nakano: *Addit. Manuf.* **36** (2020) 101624.
- 19) M. Todai, T. Nakano, T. Liu, H.Y. Yasuda, K. Hagihara, K. Cho, M. Ueda and M. Takeyama: *Addit. Manuf.* **13** (2017) 61–70.
- 20) P. Promoppatum, S.-C. Yao, P.C. Pistorius and A.D. Rollett: *Engineering* **3** (2017) 685–694.
- 21) O. Gokcekaya, T. Ishimoto, S. Hibino, J. Yasutomi, T. Narushima and T. Nakano: *Acta Mater.* **212** (2021) 116876.
- 22) T. Todo, T. Ishimoto, O. Gokcekaya, J. Oh and T. Nakano: *Scr. Mater.* **206** (2022) 114252.
- 23) T. Ishimoto, K. Hagihara, K. Hisamoto and T. Nakano: *Addit. Manuf.* **43** (2021) 102004.
- 24) T. Nakano and T. Ishimoto: *Kona Powder Particle J.* **32** (2015) 75–84.
- 25) T.J. Bruno and P.D.N. Svoronos: *CRC Handbook of Basic Tables for Chemical Analysis: Data-Driven Methods and Interpretation*, 4th ed., (CRC Press, Florida, 2020).
- 26) M. Grasso and B.M. Colosimo: *Meas. Sci. Technol.* **28** (2017) 044005.
- 27) Y. Liu, Y. Yang, S. Mai, D. Wang and C. Song: *Mater. Des.* **87** (2015) 797–806.
- 28) M.J. Zhang, G.Y. Chen, Y. Zhou, S.C. Li and H. Deng: *Appl. Surf. Sci.* **280** (2013) 868–875.
- 29) P. Wen, L. Jauer, M. Voshage, Y. Chen, R. Poprawe and J.H. Schleifenbaum: *J. Mater. Res. Technol.* **258** (2018) 128–137.
- 30) P. Wen, Y. Qin, Y. Chen, M. Voshage, L. Jauer, R. Poprawe and J.H. Schleifenbaum: *J. Mater. Res. Technol.* **35** (2019) 368–376.
- 31) D. Wang, S. Wu, F. Fu, S. Mai, Y. Yang, Y. Liu and C. Song: *Mater. Des.* **117** (2017) 121–130.
- 32) A.B. Anwar and Q.-C. Pham: *J. Mater. Process. Technol.* **240** (2017) 388–396.
- 33) H. Amano, Y. Yamaguchi, T. Sasaki, T. Sato, T. Ishimoto and T. Nakano: *J. Smart Process.* **8** (2019) 102–105.
- 34) V. Gunenthiram, P. Peyre, M. Schneider, M. Dal, F. Coste, I. Koutiri and R. Fabbro: *J. Mater. Process. Technol.* **251** (2018) 376–386.
- 35) K. Mumtaz and N. Hopkinson: *Rapid Prototyping J.* **16** (2010) 248–257.
- 36) H. Amano, Y. Yamaguchi, T. Ishimoto and T. Nakano: *Mater. Trans.* **62** (2021) 1225–1230.
- 37) S. Ly, A.M. Rubenchik, S.A. Khairallah, G. Guss and M.J. Matthews: *Sci. Rep.* **7** (2017) 4085.
- 38) J. Brillo, J. Wessing, H. Kobatake and H. Fukuyama: *J. Mol. Liq.* **290** (2019) 111226.
- 39) VDI-Gesellschaft Energietechnik: *Engineering Reference Book on Energy and Heat*, (Springer-Verlag, Berlin, 1992).
- 40) D. Dai and D. Gu: *Appl. Surf. Sci.* **355** (2015) 310–319.
- 41) X.J. Wang, L.C. Zhang, M.H. Fang and T.B. Sercombe: *Mater. Sci. Eng. A* **597** (2014) 370–375.
- 42) C. Pazon, P. Forêt, E. Hryha, T. Arunprasad and L. Nyborg: *J. Mater. Process. Technol.* **279** (2020) 116555.
- 43) H. Amano, T. Ishimoto, R. Suganuma, K. Aiba, S.-H. Sun, R. Ozasa and T. Nakano: *Addit. Manuf.* **48** (2021) 102444.
- 44) H. Gong, K. Rafi, H. Gu, G.D.J. Ram, T. Starr and B. Stucker: *Mater. Des.* **86** (2015) 545–554.
- 45) L. Xiao, W. Song, M. Hu and P. Li: *Mater. Sci. Eng. A* **764** (2019) 138204.
- 46) D. Herzog, V. Seyda, E. Wycisk and C. Emmelmann: *Acta Mater.* **117** (2016) 371–392.
- 47) J. Yang, H. Yu, J. Yin, M. Gao, Z. Wang and X. Zeng: *Mater. Des.* **108** (2016) 308–318.
- 48) T. Ahmed and H.J. Rack: *Mater. Sci. Eng. A* **243** (1998) 206–211.
- 49) A. Takase, T. Ishimoto, R. Suganuma and T. Nakano: *Scr. Mater.* **201** (2021) 113953.
- 50) S.-H. Sun, K. Hagihara, T. Ishimoto, R. Suganuma, Y.-F. Xue and T. Nakano: *Addit. Manuf.* **47** (2021) 102329.
- 51) A. Takase, T. Ishimoto, R. Suganuma and T. Nakano: *Addit. Manuf.* **47** (2021) 102257.
- 52) S. Mishra and T. DebRoy: *Acta Mater.* **52** (2004) 1183–1192.
- 53) R. Boyer, G. Welsch and E.W. Collings: *Materials Properties Handbook. Titanium Alloys*, (ASM International, Flevoland, 1994).
- 54) H. Amano, Y. Yamaguchi, T. Ishimoto and T. Nakano: *J. Smart Process.* **10** (2021) 230–234.
- 55) M. Ma, Z. Wang and X. Zeng: *Mater. Sci. Eng. A* **685** (2017) 265–273.
- 56) S.-H. Sun, T. Ishimoto, K. Hagihara, Y. Tsutsumi, T. Hanawa and T. Nakano: *Scr. Mater.* **159** (2019) 89–93.
- 57) M. Laleh, A.E. Hughes, W. Xu, N. Haghdadi, K. Wang, P. Cizek, I. Gibson and M.Y. Tan: *Corros. Sci.* **161** (2019) 108189.
- 58) Y. Tsutsumi, T. Ishimoto, T. Oishi, T. Manaka, P. Chen, M. Ashida, K. Doi, H. Katayama, T. Hanawa and T. Nakano: *Addit. Manuf.* **45** (2021) 102066.
- 59) J. Reijonen, A. Revuelta, T. Riipinen, K. Ruusuvoori and P. Puukko: *Addit. Manuf.* **32** (2020) 101030.
- 60) H. Shen, P. Rometsch, X. Wu and A. Huang: *JOM* **72** (2020) 1039–1051.
- 61) T. Ishimoto, R. Ozasa, K. Nakano, M. Weinmann, C. Schnitter, M. Stenzel, A. Matsugaki, T. Nagase, T. Matsuzaka, M. Todai, H.S. Kim and T. Nakano: *Scr. Mater.* **194** (2021) 113658.
- 62) S. Zhonggang, J. Shuwei, G. Yanhua, L. Yichen, C. Lili and X. Fei: *High Temp. Mater. Proc.* **39** (2020) 124–135.
- 63) C. Tan, K. Zhou, W. Ma, B. Attard, P. Zhang and T. Kuang: *Sci. Technol. Adv. Mater.* **19** (2018) 370–380.
- 64) A. Das, J.A. Muñoz-Lerma, E.R.L. Espiritu, A. Nommeots-Nomm, K. Waters and M. Brochu: *Sci. Rep.* **9** (2019) 13794.
- 65) C.A. Scholes and U.K. Ghosh: *Membranes* **7** (2017) 9.
- 66) T.E. Rufford, K.I. Chan, S.H. Huang and E.F. May: *Adsorpt. Sci. Technol.* **32** (2014) 49–72.